Microwave electronic spectrum of the Ne ⋯ Ne + long-range complex: The interaction potential

Alan Carrington, David I. Gammie, Josephine C. Page, Andrew M. Shaw, and Jeremy M. Hutson

Citation: The Journal of Chemical Physics **116**, 3662 (2002); doi: 10.1063/1.1436111
View online: http://dx.doi.org/10.1063/1.1436111
View Table of Contents: http://scitation.aip.org/content/aip/journal/jcp/116/9?ver=pdfcov
Published by the AIP Publishing

Microwave electronic spectrum of the $Ne\cdots Ne^+$ long-range complex: The interaction potential

Alan Carrington, David I. Gammie, Josephine C. Page, and Andrew M. Shaw[a)]
Department of Chemistry, University of Southampton, Hampshire, SO17 1BJ, United Kingdom

Jeremy M. Hutson
Department of Chemistry, University of Durham, South Road, Durham, DH1 3LE, United Kingdom

(Received 10 October 2001; accepted 27 November 2001)

The full interaction potential between $Ne(^1S)$ and $Ne^+(^2P)$ is determined by least-squares fitting of potential parameters to spectroscopic data, principally from the near-dissociation microwave spectra of the Ne_2^+ complex. The potential obtained in this way incorporates the potential curves for all six electronic states correlating with $Ne(^1S)+Ne^+(^2P)$ and the couplings between them. Coupled-channel calculations on the potential take account of breakdown of the Born–Oppenheimer approximation and provide an accurate description of the microwave rovibronic spectrum involving levels within $\sim 10\ cm^{-1}$ of the first dissociation limit. The Ne_2^+ ions are both vibrationally and rotationally hot: the spectrum involves levels up to at least $J=25/2$ and there is evidence for transitions involving levels near the second dissociation limit. The long-range levels involved have $\langle r\rangle$ up to 12 Å, compared with an equilibrium bond length of 1.756 Å for the ground electronic state. The long-range parameters of the interaction can be extracted from the fit and are compared with recent theoretical values. © *2002 American Institute of Physics.* [DOI: 10.1063/1.1436111]

INTRODUCTION

We have performed a number of microwave studies of long-range ionic complexes such as $HeAr^+$ and $HeKr^+$ in states very close to dissociation and used the results to determine accurate interaction potentials.[1,2] The near-dissociation region is characterized by a high density of states, so that electronic and vibrational transitions, as well as rotational transitions, fall in the microwave region of the electromagnetic spectrum. In addition, the Born–Oppenheimer approximation is poor near dissociation, so that conventional selection rules break down. For $HeAr^+$ and $HeKr^+$, the transition frequencies showed no obvious pattern, but we were able to assign them using a combination of double resonance experiments, Zeeman effects, and coupled-channel calculations. The spectra were then used to determine the interaction potentials involved by nonlinear least-squares fitting. Surprisingly, the interaction potentials were found to be well determined over the complete range of bond lengths, even though the microwave data involve only energy levels within a few cm^{-1} of the dissociation limit. The spectra provided information not only on the potential curves but also on the couplings between them.

We recently published the experimental energy level map resulting from the microwave electronic spectrum of $^{20}Ne_2^+$ near its first dissociation limit[3] (hereafter referred to as paper I). Because of the larger reduced mass and more strongly attractive potential of Ne_2^+, the density of states is even greater than for the He–rare gas ions and a complicated rovibronic spectrum was observed, with 276 microwave transitions involving states lying within $10\ cm^{-1}$ of the dissociation limit. An effective Hamiltonian analysis was reported, allowing the assignment of 182 of the lines. The small separation between energy levels allows the rotational Hamiltonian to mix both vibrational and electronic states, leading to pronounced breakdown of the Born–Oppenheimer approximation.

The objective of the present investigation is to use the Ne_2^+ spectra to determine the corresponding interaction potentials and thus to advance our understanding of long-range states of diatomic molecules and in particular the ways in which interaction potentials and couplings affect energy level patterns and quantum numbers. Long-range states of neutral diatomic molecules are important in many contexts, including the photoassociation of laser-cooled atoms;[4] this is particularly topical because of the recent observation of photoassociation in a Bose–Einstein condensate, producing ultracold molecules in states near dissociation.[5]

There have been a number of previous experimental investigations of the Ne_2^+ ion, principally in its ground electronic state, as listed in Table I. Early studies of the $X\,^2\Sigma_u^+$ state by dissociative recombination gave the first reliable estimate of the dissociation energy ($D_0=1.4$ eV).[6] This estimate was refined by Frommhold and Biondi,[7] who obtained $D_0=1.35\pm0.07$ eV, and by Ciurylo *et al.*,[8] who obtained $D_0=1.26\pm0.08$ eV. More recently, Hall *et al.*[9] recorded a vibrationally resolved threshold photoelectron study of Ne_2, and were able to resolve vibrational structure from 20 low-lying vibrational levels of the Ne_2^+ ion in its ground state. The Franck–Condon profile is clearly perturbed by the presence of autoionising states and the absolute vibrational assignment is uncertain because of small Franck–Condon factors to the lowest vibrational levels. Hall *et al.* considered

[a)]Author to whom correspondence should be addressed. Permanent address: School of Chemistry, University of Exeter, Stocker Road, Exeter EX4 4QD, United Kingdom.

TABLE I. Experimental and theoretical studies of Ne_2^+ ($X\,^2\Sigma^+_{1/2u}$).

Method	D_0 /eV	ω_e /cm^{-1}	$\omega_e x_e$ /cm^{-1}	Reference
Experiment				
Dissociative recombination	1.35±0.07	···	···	7
Rainbow scattering	1.30±0.1 (D_e)	···	···	22
Vacuum UV photoionization spectroscopy	1.24±0.08	···	···	23
Photofragment spectroscopy	1.35±0.1	···	···	24
Study of Rydberg states	···	586.0±2.0	5.4±0.8	10
Dissociative recombination	1.20±0.08 (D_e)	···	···	8
Photoelectron spectroscopy	1.291±0.01	569.4±3.2	7.4±0.2	9
Dissociative recombination	1.26±0.02	···	···	25
Microwave spectroscopy	1.346	587.8	7.71	This work
Theory				
SCF	1.61	660	···	26
CI	1.20	550.1	7.1	27
Density-functional method	1.310	597.0	6.1	28
UMP4	1.258	···	···	29
MRCCI+Q	1.32	598.5	8.2	24
QCISD(t)	1.376 (D_e)	591	···	30
MR MBPT	1.283	588.3	8.7	31
RCCSD-T	1.376	605.2	8.0	11

two vibrational assignments, and gave analyses based on assigning the first observed component as either $v=0$ or $v=2$; the $v=2$ assignment was considered because it gave a value of D_0 that was closer to those observed previously. The value obtained for ω_e depends on the vibrational assignment. Kim *et al.*[10] carried out complementary studies of Rydberg states converging on the Ne_2^+ ionic core in $v=0$, 1, and 2 states and confirmed their vibrational assignment by isotopic studies; the resulting value of ω_e, $586\pm2\ \mathrm{cm}^{-1}$, suggests that the lowest level observed by Hall *et al.* was actually $v=3$. The value of $\omega_e x_e$ obtained by Hall *et al.*,[9] $7.42\pm0.16\ \mathrm{cm}^{-1}$, is probably the more reliable because they observed many more vibrational levels.

There have also been a number of electronic structure calculations of the interaction potentials for Ne_2^+, at various levels of accuracy. Table I summarizes these, and gives the resulting binding energies and vibrational parameters. The most recent of the calculations are those of Naumkin and Wales,[11] who were motivated by an interest in the structure of ionic Ne clusters and the role of Ne_2^+ or Ne_3^+ as the core species of larger clusters. Naumkin and Wales performed open-shell coupled-cluster RCCSD(T) calculations on Ne_2^+ with an aug-cc-pVQZ basis set, designed as the preparatory step for a diatomics-in-molecules study of charged neon clusters.

The interaction potential for Ne $(^1S)+\mathrm{Ne}^+(^2P)$ is best described in terms of separated atom states. In Ne_2^+, the orbital angular momentum of Ne^+ quantizes along the interatomic axis to form Σ and Π states; because of the homonuclear symmetry, and in the absence of spin–orbit coupling, there are four states that are degenerate at dissociation, labeled Σ_g, Π_g, Σ_u, and Π_u. Addition of spin–orbit coupling splits the atomic ^2P state of Ne^+, and thus the dissociation limit of Ne_2^+, into components with total atomic (orbital+spin) angular momentum $J_a=1/2$ and 3/2. For Ne^+, the $^2P_{1/2}$ excited state lies $\Delta=782\ \mathrm{cm}^{-1}$ above the $^2P_{3/2}$ ground state. The spin–orbit coupling splits and mixes the Σ and Π states of Ne_2^+ into six states: $\Omega=1/2$ and $\Omega=3/2$ states of g and u symmetry correlating with the dissociation limit $\mathrm{Ne}^+(^2P_{3/2})+\mathrm{Ne}(^1S)$, and $\Omega=1/2$ states of g and u symmetry correlating with the limit $\mathrm{Ne}^+(^2P_{1/2})+\mathrm{Ne}(^1S)$. Curves calculated from the *ab initio* results of Naumkin and Wales[11] are shown in Fig. 1. At long range, all the curves are dominated by the attractive $C_4 r^{-4}$ charge-induced dipole interaction.

The present paper reports the fitting of interaction poten-

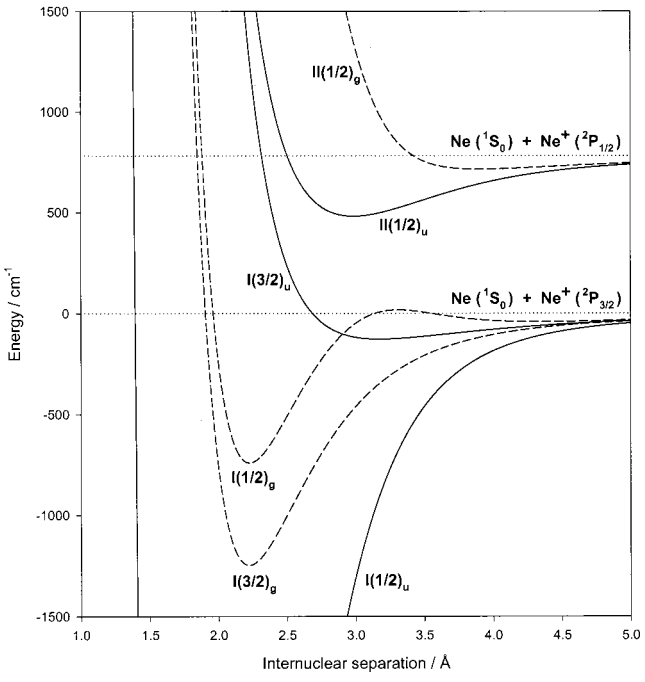

FIG. 1. The potential energy curves for Ne_2^+.

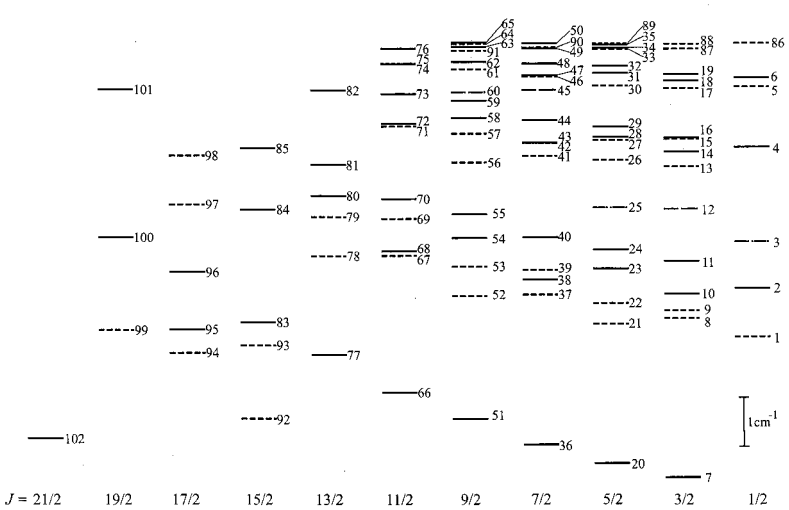

FIG. 2. The energy level diagram at the first dissociation limit. Dashed lines (---) indicate *g* symmetry levels and solid lines indicate levels of *u* symmetry.

tials to the experimental data presented in paper I. Most of the 94 transitions previously unassigned have been identified and included in the fit. The new assignments have been confirmed with double resonance or Zeeman experiments.

REPRESENTATION OF THE INTERACTION POTENTIAL

In our previous investigations of $HeAr^+$ (Ref. 1) and $HeKr^+$,[2] we were able to find a simple functional form for the interaction potential, incorporating correct isotropic and anisotropic interactions at long range, which was adequate to explain all the spectra. However the ground electronic states of these complexes have well depths of 282 cm^{-1} and 208 cm^{-1}, respectively, whereas the well depth of the Ne_2^+ ion in its ground state is around 10 800 cm^{-1}. Representing such a deep potential in a way that is satisfactory at both short and long range presents a greater challenge.

The electronic Schrödinger equation for the homonuclear species Ne_2^+ separates into two independent problems of *g* and *u* electronic symmetry. The interaction potentials for *g* and *u* states are therefore represented separately. However, the long-range coefficients for *g* and *u* states should be the same; the two fits thus provide different determinations of the long-range parameters, and comparing them allows us to assess the accuracy of the results.

The interaction potential between a closed-shell atom and one in a *P* state may be represented in two ways, in terms of V_Σ and V_Π or in terms of V_0 and V_2. The two representations are equivalent and interchangeable,

$$V_\Sigma(r) = V_0(r) + \tfrac{2}{5}V_2(r),$$
$$V_\Pi(r) = V_0(r) - \tfrac{1}{5}V_2(r). \tag{1}$$

In Refs. 1 and 2, we chose to parameterize V_0 and V_2 rather than V_Σ and V_Π because the V_0 and V_2 curves were qualitatively different: V_2 is much smaller than V_0, and decays as r^{-6} rather than r^{-4} at long range; for $HeAr^+$ and $HeKr^+$, it has no sign change as a function of *r*. However, initial fitting for Ne_2^+ showed that (for the *g* states) V_0 and V_2 are of comparable magnitude in the well region and both have deep potential minima. Under these circumstances it is more convenient to parameterize the spin-free Σ and Π curves rather than V_0 and V_2. The two representations are easily exchanged when necessary at a given *r* using Eq. (1), though the curves have a simple functional form only in the representation used for the parameterization.

It is often conceptually useful to display adiabatic curves including spin–orbit coupling, as in Fig. 1. For low-lying vibrational states, where the Born–Oppenheimer approximation is good, these are the curves that determine the energy level pattern. They may be obtained by diagonalizing the 3×3 matrix of $V(r,\theta_a) + H_{\text{spin-orbit}}$ in either a Hund's case (a) or a Hund's case (c) basis set. In the present work, the spin–orbit coupling operator is assumed to be the same in the Ne_2^+ molecule as in the Ne^+ atomic ion and thus to show no significant variation with *r*. This approximation should be good at long range, in the region probed by the near-dissociation spectra, and proved adequate in the present work. It would however be interesting to test it using *ab initio* calculations with spin–orbit coupling included explicitly. The resulting curves are

$$V_{I_{1/2}}(r) = \frac{V_\Sigma(r) + V_\Pi(r)}{2} + \frac{\Delta}{2} - D(r),$$
$$V_{II_{3/2}}(r) = V_\Pi(r), \tag{2}$$
$$V_{II_{1/2}}(r) = \frac{V_\Sigma(r) + V_\Pi(r)}{2} + \frac{\Delta}{2} + D(r),$$

where Δ is the splitting between the atomic spin–orbit states and

$$D(r) = \tfrac{1}{2}\sqrt{\Delta^2 + [V_\Sigma(r) - V_\Pi(r)]^2 - \tfrac{2}{3}\Delta[V_\Sigma(r) - V_\Pi(r)]}. \tag{3}$$

Each set of adiabatic potentials is constructed separately for the states of *g* and *u* electronic symmetry (Figs. 2 and 3).

In our previous studies of $HeAr^+$ and $HeKr^+$, we employed a Morse function to describe the short-range part of the potential, supplemented with both isotropic and aniso-

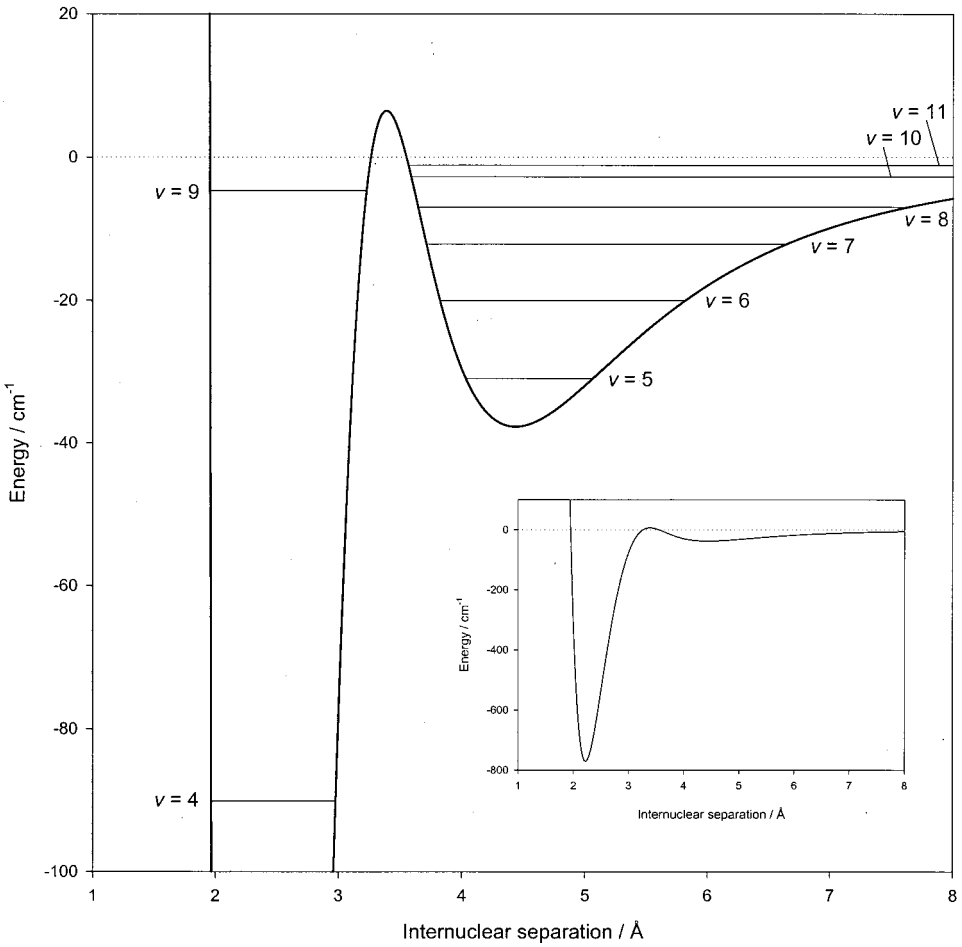

FIG. 3. Detail of the inner well potential on the $I(1/2)_g$ state.

tropic long-range contributions. The same functional form is employed here for the spin-free potentials for Ne_2^+,

$$V_\Lambda(r)=A_\Lambda(1-a_\Lambda)\exp[-\beta_\Lambda(r-r_{e\Lambda})] + A_\Lambda a_\Lambda \exp\left[-\frac{1}{2}\beta_\Lambda(r-r_{e\Lambda})\right] - \sum_{n=4,6,8,10}\frac{[C_n]_\Lambda D_{n\Lambda}(r)}{r^n}, \quad (4)$$

where $D_{n\Lambda}(r)$ are Tang–Toennies damping functions[12] that prevent the long-range terms dominating at short r and have the functional form,

$$D_{n_\Lambda}(r)=1-\exp(-\beta_\Lambda r)\sum_{m=0}^{n}\frac{(\beta_\Lambda r)^m}{m!}. \quad (5)$$

The subscript Λ takes the values Σ_g, Π_g, Σ_u, and Π_u.

At long range, the interaction between Ne and Ne^+ is weak compared to the atomic spin–orbit coupling. Under these circumstances, the atomic L and S quantum numbers remain coupled to form a resultant J_a, as in the free Ne^+ atom. There are then two possibilities for how the rotational motion of the diatomic molecule is included. In Hund's case (c), the projection Ω of J_a onto the internuclear axis is a good quantum number. There is no quantum number for the end-over-end rotation itself. Instead, only the total angular momentum J is defined; like J_a, J has projection Ω onto the internuclear axis. The alternative to this is case (e), where a mechanical rotation quantum number R is defined but Ω is not. In case (e), J_a couples to R to give a resultant J. Case (e) is thus an entirely space-fixed coupling scheme, with no molecule-fixed projection quantum numbers. ^{20}Ne has nuclear spin $I=0$, so there is no hyperfine structure.

In practice, the energy level patterns of real systems near dissociation are intermediate between case (c) and case (e). As seen above, it is convenient to label potential curves with values of Ω. In general, case (c) is observed when the energy associated with molecular rotation is small compared to the separation between levels with the same J_a but different Ω. Conversely, case (e) is observed when the rotational energy is large compared to the separation. In previous work,[1,2] we found that $HeAr^+$ was best described by case (c) quantum numbers (with significant rotational couplings), whereas $HeKr^+$ was remarkably close to pure case (e). Ne_2^+ is intermediate between the two in this respect, with levels that are best described by case (c) quantum numbers at low J but come closer to case (e) at high J.

The dominant long-range term in the interaction potential is the charge/induced-dipole interaction $(-C_4 r^{-4})$, whose coefficient is determined by the dipole polarizability of the Ne atom.[13] This interaction is isotropic, so the coefficient takes the same value for Σ and Π states; its value was fixed at $C_4=1.335\,E_h a_0^4$ during the fitting process. The disposable parameters of Eq. (5) for each potential curve are

thus A_Λ, β_Λ, $[C_6]_\Lambda$, $[C_8]_\Lambda$, and $[C_{10}]_\Lambda$. It would in principle be possible to fit to these parameters directly, but our previous investigations of the potentials for $HeAr^+$ and $HeKr^+$ showed that the parameters of such a fit are highly correlated. The correlation problem is reduced by rearranging the parameters of the potential, replacing A_Λ and $[C_8]_\Lambda$ with the well depth ε_Λ and the equilibrium bond length, $r_{e\Lambda}$. The procedure for finding the values of A_Λ and $[C_8]_\Lambda$ needed to give specified values of ε_Λ and $r_{e\Lambda}$ has been described elsewhere.[1] Further reductions in parameter correlation are achieved by holding the parameters $[C_{10}]_\Lambda$ fixed so that the ratio of C_{10}/C_8 (γ in this parameter set) is set at the value predicted by the single-oscillator formula of Thakkar and Smith.[14] In the present work, the C_{10}/C_8 ratio for Ne_2^+ was fixed at 11 a_0^2, a value based on the lower bounds of the C_6 and C_8 coefficients of neutral Ne_2 from Standard and Certain.[15]

The isotropic coefficient $[C_6]_0$ in the long-range expansion has a contribution from both the charge/induced-quadrupole interaction and the isotropic dispersion interaction. The quadrupole polarizability of the Ne atom is known[15] and a simple Slater–Kirkwood[16] calculation of the dispersion interaction allows $[C_6]_0$ to be estimated as 7.69 $E_h a_0^6$. The anisotropic contributions are more difficult to estimate, with contributions from atomic quadrupole/induced-dipole and anisotropic dispersion interactions. At the start of this work, a value for the quadrupole moment of Ne^+ was available ($\Theta_{Ne^+} = 1.122 e a_0^2$),[17] and an estimate of the induction contribution could be made. The anisotropic contribution to the dispersion was not known but was thought to be smaller and of opposite sign to the induction term. From these considerations, we estimated the upper and lower bounds on the $[C_6]$ coefficients as $7.69 < [C_6]_\Sigma < 11.29$ $E_h a_0^6$ and $5.89 < [C_6]_\Pi < 7.69$ $E_h a_0^6$.

THE LEAST-SQUARES FIT OF THE INTERACTION POTENTIAL

The potentials for *g* and *u* symmetries were fitted independently of one another. At each stage of the fit, energy levels for the trial potential were calculated using the coupled-channel method as implemented in the program BOUND,[18] including all channels correlating with the $^2P_{1/2}$ and $^2P_{3/2}$ states of Ne^+. Such a calculation includes the couplings between electronic and spin-orbit states and thus takes full account of deviations from the Born–Oppenheimer approximation. In the present work, the coupled-channel calculations were performed in a case (e) representation for reasons of computational convenience, as described previously.[1] A fully-coupled calculation in a case (c) basis set would have given identical results. Derivatives of the spectroscopic frequencies with respect to potential parameters were calculated by finite differences, and nonlinear least-squares fitting was carried out using the I-NOLLS package.[19] I-NOLLS is an interactive least-squares fitting package that gives the user detailed control over the progress of the fit, with the ability to inspect statistical information, switch between alternative spectroscopic assignments and add or remove experimental data and fitting parameters as the fit proceeds.

TABLE II. The parameters of the final interaction potential.

		g states		*u* states	
Parameter	Units	Value	95% conf.	Value	95% conf.
ε_Σ	mE_h	0.128 117	0.000 365	51.997 130	0.674 786
ε_Π	mE_h	5.792 196	0.014 511	0.510 428	0.032 491
$r_{e\Sigma}$	a_0	9.212 993	0.006 860	3.195 730	0.072 518
$r_{e\Pi}$	a_0	4.193 729	0.004 235	6.315 226	0.111 942
β_Σ	$(a_0)^{-1}$	2.417 502	0.008 527	2.305 779	0.048 446
β_Π	$(a_0)^{-1}$	2.476 164	0.022 252	2.549 226	0.599 878
C_4	$E_h a_0^4$	1.335	(Fixed)	1.335	(Fixed)
$[C_6]_\Sigma$	$E_h a_0^6$	9.112 339	1.569 079	11.371 651	6.998 988
$[C_6]_\Pi$	$E_h a_0^6$	5.955 124	0.907 559	6.257 588	3.323 900
A_Σ	mE_h	0.081 623	(Derived)	−5.291 854	(Derived)
A_Π	mE_h	−1.184 987	(Derived)	0.499 013	(Derived)
$[C_8]_\Sigma$	$E_h a_0^8$	438.7067	(Derived)	−419.6579	(Derived)
$[C_8]_\Pi$	$E_h a_0^8$	−56.2157	(Derived)	203.3153	(Derived)
γ	a_0^2	11.0	(Fixed)	11.0	(Fixed)
a_Σ	⋯	1.000 000 0	(Fixed)	1.878 186	0.671 526
a_Π	⋯	4.846 694	3.070 511	0.879 177	0.169 900

The choice of which near-dissociation energy level data to include in the fit is important to the quality of the fit and the rate at which it converges. Spacings between energy levels on the experimental energy level diagram were selected to represent separations between vibrational levels, rotational progressions, Ω-doubling-type separations and separations between electronic states for both high and low *J*. This provided a balanced set of level separations that was calculated from the trial potentials at each iteration of the fit.

To obtain starting points for the fits to experimental data, the functional form of Eq. (4) was first fitted to the *ab initio* calculations of Naumkin and Wales.[11] Unfortunately, the uncertainties in the *ab initio* well depths leave room for some ambiguity in the absolute vibrational assignments. For levels at the bottom of the well, this can be resolved using the results of Kim *et al.*[10] described above. Spectroscopic fits to the microwave data are nevertheless possible for several slightly different quantum number assignments near dissociation. In the present work, this was resolved for the *u* states by including the ω_e value of Kim *et al.*[10] and the $\omega_e x_e$ value of Hall *et al.*[9] in preliminary fits. This provided a number of possible vibrational assignments for the *u*-state levels for both $\Omega = 1/2$ and $\Omega = 3/2$.

Suitable starting points for fitting to the *g*-state potentials were harder to find, and as a result there was less uncertainty in the vibrational assignments. In paper I, the rotational constant for one progression of levels was found to be considerably larger than for others near it in energy; this arises because there is a double minimum in the potential for the $I(1/2)_g$ state, and both inner-well and outer-well levels exist. The presence of the inner-well levels proved to be a very useful constraint. Finding a starting point that provided an inner-well level in the energy region near dissociation was extremely difficult and only one vibrational assignment proved to be satisfactory for the *g*-state levels.

In our earlier work on $HeAr^+$ and $HeKr^+$, Zeeman *g*-factors were included in the data set used for fitting the

TABLE III. Experimental data required to construct Fig. 2 and comparison with transition frequencies calculated from the final potential.

Frequency /MHz	Calculated/ MHz	Obs.−Calc. /MHz	Level number	J	Level number	J	Frequency /MHz	Calculated/ MHz	Obs.−Calc. /MHz	Level number	J	Level number	J
8 702.4	8 687.6	14.8	15	3/2	29	5/2	41 099.4	41 107.8	−7.9	52	9/2	54	9/2
9 448.7	9 410.9	38.0	27	5/2	29	5/2	41 752.3	41 496.4	256.1	52	9/2	40	7/2
14 520.2	14 473.1	47.1	39	7/2	24	5/2	42 229.5	42 094.5	134.6	12	3/2	23	5/2
15 590.9	15 580.4	10.5	9	3/2	2	1/2	43 047.2	42 823.8	223.4	78	13/2	80	13/2
16 875.0	16 995.6	−121.0	45	7/2	32	5/2	43 747.0	43 855.3	−108.3	12	3/2	4	1/2
17 021.2	17 073.5	−54.4	33	5/2	31	5/2	45 576.8	45 687.9	−110.7	5	1/2	14	3/2
17 257.8	17 257.6	0.2	8	3/2	10	3/2	45 748.3	46 517.0	−768.6	57	9/2	70	11/2
17 270.7	17 627.4	−356.7	61	9/2	73	11/2	45 983.2	46 003.3	−20.5	25	5/2	43	7/2
17 870.3	17 793.7	76.5	42	7/2	58	9/2	48 053.9	47 701.7	352.7	56	9/2	73	11/2
18 186.1	18 252.0	−65.2	37	7/2	23	5/2	48 419.5	47 674.1	745.2	53	9/2	70	11/2
19 445.8	19 477.2	−31.4	45	7/2	58	9/2	48 597.9	47 425.5	1172.4	79	13/2	85	15/2
19 804.4	19 798.9	3.2	60	9/2	74	11/2	49 439.1	49 478.2	−39.2	25	5/2	16	3/2
20 087.1	20 046.4	40.1	60	9/2	48	7/2	51 082.9	51 224.4	−141.5	12	3/2	28	5/2
20 913.3	20 890.7	22.6	21	5/2	10	3/2	58 023.5	57 731.9	292.0	52	9/2	55	9/2
21 019.9	21 084.3	−65.1	64	9/2	47	7/2	58 973.5	59 085.8	−112.2	13	3/2	24	5/2
21 148.0	20 841.5	306.5	53	9/2	40	7/2	61 055.9	61 124.1	−67.9	25	5/2	10	3/2
21 165.7	21 115.5	50.1	60	9/2	62	9/2	61 066.2	61 074.6	−7.5	56	9/2	47	7/2
21 238.9	21 598.6	−359.7	75	11/2	73	11/2	61 664.2	61 539.3	124.9	25	5/2	44	7/2
21 244.7	21 234.7	10.0	8	3/2	2	1/2	69 492.7	70 969.1	−1476.4	67	11/2	77	13/2
21 986.4	22 011.2	−25.0	60	9/2	72	11/2	74 490.9	76 703.2	−2120.1	79	13/2	83	15/2
22 742.3	22 451.9	290.3	71	11/2	73	11/2	87 620.0	88 347.2	728.1	37	7/2	51	9/2
23 161.3	23 159.1	2.3	26	5/2	29	5/2	93 829.6	93 916.8	−87.7	25	5/2	19	3/2
23 166.9	23 270.0	−102.8	46	7/2	35	5/2	95 738.3	95 935.8	−197.5	12	3/2	31	5/2
23 233.7	23 023.1	210.2	69	11/2	68	11/2	99 592.7	99 958.0	−365.3	22	5/2	36	7/2
23 418.6	23 181.7	237.2	39	7/2	40	7/2	113 060.8	113 410.3	−349.5	46	7/2	40	7/2
24 184.3	24 224.2	−39.8	22	5/2	23	5/2	113 594.9	113 708.7	−114.6	3	1/2	18	3/2
24 434.1	24 324.1	110.2	79	13/2	68	11/2	113 787.0	113 953.7	−166.6	17	3/2	24	5/2
25 226.5	24 991.2	235.3	71	11/2	82	13/2	115 813.7	115 917.4	−103.7	3	1/2	6	1/2
25 781.7	25 737.8	44.1	45	7/2	29	5/2	117 002.6	116 759.4	243.2	9	3/2	7	3/2
26 692.5	26 624.8	67.9	41	7/2	58	9/2	118 423.0	118 441.4	−18.3	37	7/2	20	5/2
26 881.5	27 334.1	−452.6	71	11/2	81	13/2	123 866.0	125 106.1	−1240.1	79	13/2	66	11/2
27 306.9	27 301.5	5.86	56	9/2	72	11/2	123 877.5	123 924.5	−47.0	30	5/2	11	3/2
29 178.0	29 360.8	−183.0	45	7/2	49	7/2							
29 195.4	29 195.0	0.4	60	9/2	63	9/2	Transitions observed from fit predictions.						
29 392.1	29 431.1	−39.0	22	5/2	11	3/2	11 259.6	11 524.6	−265.6	93	15/2	95	17/2
29 613.7	29 806.1	−192.9	45	7/2	34	5/2	22 621.4	22 649.9	−28.6	87	3/2	18	3/2
29 718.9	29 415.3	303.6	67	11/2	55	9/2	19 107.5	19 156.7	−49.9	90	7/2	47	7/2
29 875.8	29 834.8	41.0	42	7/2	59	9/2	21 315.0	19 289.6	2025.1	94	17/2	83	15/2
29 989.7	30 061.8	−72.4	30	5/2	50	7/2	22 239.5	22 275.3	−35.4	88	3/2	19	3/2
30 591.3	30 522.1	69.1	60	9/2	76	11/2	22 348.1	22 381.1	−32.4	89	5/2	19	3/2
30 856.7	30 913.8	−56.7	21	5/2	38	7/2	25 744.3	24 629.3	1115.0	86	1/2	6	1/2
31 348.2	31 203.9	144.9	56	9/2	58	9/2	26 171.7	26 563.1	−441.4	91	9/2	73	11/2
31 600.7	31 772.5	−171.5	52	9/2	68	11/2	40 476.2	38 652.2	1823.9	99	19/2	96	17/2
32 812.1	32 819.1	−7.0	3	1/2	2	1/2	45 284	43 984.6	1299.2	92	15/2	77	13/2
32 852.5	32 774.9	77.6	45	7/2	28	5/2	46 207.2	44 833.2	1324.7	98	17/2	101	19/2
33 085.5	33 351.6	−266.1	78	13/2	84	15/2	48 030.2	49 685.9	−1655.7	97	17/2	96	17/2
33 260.8	33 446.5	−185.9	45	7/2	65	9/2	58 000.7	61 085.1	−3084.6	98	17/2	100	19/2
34 138.6	34 105.7	32.9	1	1/2	2	1/2	76 493.7	81 608.7	−5114.8	99	19/2	102	21/2
39 575.6	39 564.5	11.1	25	5/2	14	3/2	83 434.7	83 073.5	97.7	97	17/2	83	15/2
40 215.4	40 287.3	−71.6	8	3/2	11	3/2	88 184.4	88 085.5	98.5	97	17/2	95	17/2
40 641.0	40 376.1	265.8	37	7/2	40	7/2	118 037.5	120 255.1	−2220.7	98	17/2	83	15/2
40 907.6	40 243.7	663.9	78	13/2	70	11/2							

potentials. For Ne_2^+, however, the g-factors were found to be insensitive to detailed variation of the potential parameters. They remained a useful check of the quality of the fit and in particular the accuracy of the level assignment.

As described above, several different vibrational assignments were explored for the u states, and three of them produced reasonable minima in the target function χ^2 (the weighted sum of squares) for the chosen experimental data. To distinguish between the three resulting potentials, levels up to $J=31/2$ were calculated for each potential and compared with the initially unassigned transition frequencies. This allowed a single potential to be selected. Guided by the predictions of the fit, a further 12 levels of g symmetry and 5 of u symmetry were identified and their positions were confirmed by double resonance. Refining the fit then provided assignments for all but 31 of the remaining transitions within the error of the fit (297 MHz). We know from Zeeman studies that some of the remaining transitions correlate with the

TABLE IV. Correlation matrices for fits to the potentials for the u states (lower triangle) and g states (upper triangle).

u/g	ε_Σ	ε_Π	$r_{e\Sigma}$	$r_{e\Pi}$	β_Σ	β_Π	$[C_6]_\Sigma$	$[C_6]_\Pi$	a_Σ	a_Π
ε_Σ	u/g	−0.601	−0.035	0.348	0.277	0.323	−0.439	0.511	⋯	−0.490
ε_Π	0.515	u/g	−0.569	−0.280	0.422	0.061	−0.226	−0.104	⋯	0.368
$r_{e\Sigma}$	0.691	0.595	u/g	0.392	−0.772	−0.213	0.566	−0.011	⋯	−0.011
$r_{e\Pi}$	−0.942	−0.692	−0.660	u/g	0.209	−0.235	0.016	0.035	⋯	0.067
β_Σ	0.691	0.644	0.978	−0.700	u/g	−0.091	−0.782	−0.090	⋯	0.261
β_Σ	−0.417	0.525	0.037	0.236	0.049	u/g	0.072	0.941	⋯	−0.876
$[C_6]_\Sigma$	−0.747	−0.514	−0.846	0.724	−0.801	0.105	u/g	0.003	⋯	−0.297
$[C_6]_\Pi$	−0.400	−0.208	−0.079	0.463	0.128	0.162	0.243	u/g	⋯	−0.865
A_Σ	−0.506	−0.596	−0.959	0.529	−0.967	−0.200	0.777	−0.235	u/g	⋯
A_Π	−0.885	−0.167	−0.408	0.813	−0.431	0.751	0.523	0.379	0.219	u/g

second $J_a=1/2$ dissociation limit, so the presence of unassigned lines is to be expected. For example, the Zeeman effect for the transition at 23 101.6 MHz suggests that it is a $J=3/2-3/2$ transition with g-factors corresponding to the $J_a=1/2$ dissociation limit.

The parameters of the final potential that gave the best predictions are presented in Table II. The comparison between observed and calculated transition frequencies, including the newly assigned transitions, is given in Table III. The correlation matrix for the fit is given in Table IV. For both g and u states, the parameters are highly correlated.

The root mean square (rms) deviation for the set of 84 level separations included in the final fits is 218 MHz. Most of the error arises from the poor determination of the position of the lowest observed $\Omega=3/2_u$ vibration progression. The error in the transition frequencies to levels in this progression is of the order of 1 GHz. Although the separations between the levels, and hence the rotational spacings, are well reproduced by the interaction potential, the absolute binding energy is poorly determined.

DISCUSSION

Some properties of the electronic states of Ne_2^+, as determined by the fitted potential parameters, are presented in Table V. Our ground-state potential has a well depth of 11 244.9 cm^{-1} and supports 44 vibrational energy levels. However, the absolute quantum number assignment of the near-dissociation levels is not conclusively determined, and the true well depth could differ from this by a few percent. A well depth of this size places considerable demands on the representation of the interaction potential over the entire range of bond lengths. At short range there is significant overlap of the atomic wave functions and, for the ground state, this results in a weak chemical bond. A simple Morse function is used to describe this part of the potential in the present work, with Tang–Toennies damping functions preventing the r^{-n} expansion from dominating at short range. Such functional forms have been used previously for systems with potential well depths[1,2] of order a few hundred cm^{-1}, but they may not be adequate for a detailed description of the deeper potential well in Ne_2^+. An alternative possibility that we considered was to start from a pointwise representation of the potential, from *ab initio* calculations, and to morph it as described by Meuwly and Hutson;[20] such an approach would give an efficient representation of the shape in the well region, but we decided that we preferred to have an explicit representation of the leading long-range contributions.

We have determined empirical values of the C_6 coefficients for each of the four spin-free electronic states, and it is interesting to compare them with theoretical values. Medved *et al.*[21] have recently calculated the quadrupole moments and the dipole polarizabilities of a range of ^2P atoms, including Ne^+, and have estimated the isotropic and anisotropic coefficients for Ne_2^+. Their values are $[C_6]_0=6.86\ E_h a_0^6$ and $[C_6]_2=8.71\ E_h a_0^6$. For Ne_2^+, $[C_6]_0$ has approximately equal contributions from dispersion and quadrupolar induction, whereas $[C_6]_2$ is dominated by the atomic quadrupole/induced dipole term. The coefficients for Σ and Π states are related to $[C_6]_0$ and $[C_6]_2$ through equations analogous to Eqs. (1) above, and are the same for g and u states. The resulting theoretical values may be compared with those obtained from the fits to experimental data: for the Σ states, $[C_6]_g=9.112(1.563)$; $[C_6]_{calc}=10.354$; $[C_6]_u=11.372(6.999)$, and for the Π states, $[C_6]_g=5.955(0.908)$; $[C_6]_{calc}=5.128$; $[C_6]_u=6.258(3.324)$ (all in $E_h a_0^6$, with 95% confidence limits in parentheses). The empirical values thus agree with the theoretical values to

TABLE V. Characteristics of fitted potentials for the g and u electronic states.

State/ [case (c)]	D_e/cm^{-1}	r_e/Å	Number of vibrational levels	ω_e/cm^{-1}	B/cm^{-1} $v=0$	$\omega_e x_e$/cm^{-1}
I $(1/2)_u$	11244.9	1.765	44	587.8	0.5849	7.71
I $(1/2)_g$	765.3	2.212	14	194.3	0.3337	9.34
I $(3/2)_u$	112.0	3.337	10	33.8	0.1421	3.10
I $(3/2)_g$	1270.4	2.215	25	196.9	0.3351	8.46
II $(1/2)_u$	261.0	3.10	⋯	⋯		⋯
II $(1/2)_g$	63.0	3.90	⋯	⋯		⋯

TABLE VI. Comparison of rotational constants B from the effective Hamiltonian fit of paper 1 with those from expectation values calculated from the best-fit potential.

B/MHz	$v=39$ I $(1/2)_u$	$v=6$ I $(3/2)_u$	$v=40$ I $(1/2)_u$	$v=7$ I $(3/2)_u$	$v=41$ I $(1/2)_u$	$v=8$ I $(3/2)_u$
Effective H	1347.2	1368.2	928.9	946.3	579.7	591.9
Expectation value	1353.4	1333.6	932.9	926.9	584.5	576.6

within the experimental errors (which are large in some cases).

Once the potential is known, properties such as binding energies and expectation values can be calculated for the long-range states involved in the microwave spectrum. For example, level 62 is the most weakly bound level of *u* symmetry, and has $J=9/2$; calculations on the best-fit potential assign it a binding energy of 1.2 GHz and an average bond length $\langle r\rangle = 12$ Å from the coupled-channel calculations. Comparisons can also be made between the average bond lengths derived from the effective Hamiltonian analysis of paper I and those obtained from direct calculation of $\langle 1/r^2\rangle$ on the best-fit potential. If Coriolis effects are neglected, rotational constants can be estimated from $B=\langle \hbar^2/2\mu r^2\rangle$, where μ is the molecular reduced mass. Results for $J=1/2$ levels of the $\Omega=1/2$ states and $J=3/2$ levels of the $\Omega=3/2$ states are given in Table VI.

CONCLUSIONS

We have determined interaction potentials for Ne_2^+ by least-squares fitting to experimental data, mostly near-dissociation microwave spectra. The representation of the interaction potential for Ne_2^+ was considerably more difficult than for $HeAr^+$ and $HeKr^+$, which we studied previously. In the earlier systems, the near-dissociation microwave spectra were able to determine the potential uniquely over the entire range of internuclear separations. For Ne_2^+, with a much larger well depth, there is some ambiguity remaining and the absolute vibrational assignment cannot yet be determined uniquely. However, the most satisfactory solution gives a ground-state potential that supports 44 vibrational levels. With this assignment, 245 of the 276 transitions observed in the microwave electronic spectrum have been assigned.

ACKNOWLEDGMENTS

A.C. thanks the Royal Society for a Research Professorship, D.I.G. thanks the Royal Society for a studentship, J.C.P. thanks the EPSRC for a Studentship, and A.M.S. thanks the University of Southampton for a Research Fellowship. This work is supported by the Royal Society and the EPSRC.

[1] A. Carrington, C. A. Leach, A. J. Marr, A. M. Shaw, M. R. Viant, J. M. Hutson, and M. M. Law, J. Chem. Phys. **102**, 2379 (1995).
[2] A. Carrington, C. H. Pyne, A. M. Shaw, S. M. Taylor, J. M. Hutson, and M. M. Law, J. Chem. Phys. **105**, 8602 (1996).
[3] A. Carrington, D. I. Gammie, J. C. Page, A. M. Shaw, and S. M. Taylor, Phys. Chem. Chem. Phys. **1**, 29 (1999).
[4] W. C. Stwalley and H. Wang, J. Mol. Spectrosc. **195**, 194 (1999).
[5] R. Wynar, R. S. Freeland, D. J. Han, C. Ryu, and D. J. Heinzen, Science **287**, 1016 (2000).
[6] T. R. Connor and M. A. Biondi, Phys. Rev. A **140**, A778 (1965).
[7] L. Frommhold and M. A. Biondi, Phys. Rev. **185**, 244 (1969).
[8] R. Ciurylo, A. Bielski, J. Domystawska, J. Szudy, and R. S. Trawiński, J. Phys. B **27**, 4181 (1994).
[9] R. I. Hall, Y. Lu, T. Matsui, T. Tanaka, H. Yoshii, T. Hayaishi, and K. Ito, J. Phys. B **28**, 2435 (1995).
[10] S. B. Kim, D. J. Kane, and J. G. Eden, Phys. Rev. Lett. **68**, 1311 (1992).
[11] F. Y. Naumkin and D. J. Wales, Mol. Phys. **93**, 633 (1998).
[12] K. T. Tang and J. P. Toennies, J. Chem. Phys. **80**, 3726 (1984).
[13] *CRC Handbook of Physics and Chemistry*, 75th ed., edited by D. R. Lide (CRC, Boca Raton, 1994).
[14] A. J. Thakkar and V. H. Smith, Jr., J. Phys. B **7**, L321 (1974).
[15] J. M. Standard and P. R. Certain, J. Chem. Phys. **83**, 3002 (1985).
[16] J. O. Hirschfelder, C. F. Curtiss, and R. B. Bird, *Molecular Theory of Liquids and Gases* (Wiley, New York, 1954).
[17] E. S. Chang and H. Sakai, J. Phys. B **15**, L649 (1982).
[18] J. M. Hutson, BOUND computer program, version 5, distributed by Collaborative Computational Project No. 6 of the UK Engineering and Physical Sciences Research Council, 1993.
[19] M. M. Law and J. M. Hutson, Comput. Phys. Commun. **102**, 252 (1997).
[20] M. Meuwly and J. M. Hutson, J. Chem. Phys. **110**, 8338 (1999).
[21] M. Medved, P. W. Fowler, and J. M. Hutson, Mol. Phys. **98**, 453 (2000).
[22] H. U. Mittman and H. P. Weise, Z. Naturforsch. A **29A**, 400 (1974).
[23] D. J. Trevor, J. E. Pollard, W. D. Brewer, S. H. Southworth, C. M. Truesdale, D. A. Shirly, and Y. T. Lee, J. Chem. Phys. **80**, 6083 (1984).
[24] L. Broström, M. Larsson, S. Mannervik, R. T. Short, and D. Sonnek, J. Chem. Soc., Faraday Trans. **87**, 797 (1991).
[25] G. Ramos, J. W. Sheldon, K. A. Hardy, and J. R. Peterson, Phys. Rev. A **56**, 1913 (1997).
[26] T. L. Gilbert and A. C. Wahl, J. Chem. Phys. **55**, 5247 (1971).
[27] J. S. Cohen and B. Schneider, J. Chem. Phys. **61**, 3230 (1974).
[28] H. H. Michels, R. H. Hobbs, and L. A. Wright, J. Chem. Phys. **69**, 5151 (1978).
[29] G. Fenking, W. Koch, D. Cremer, J. Gauss, and J. F. Liebman, J. Phys. Chem. **93**, 3410 (1989).
[30] G. E. Löpez, J. Comput. Chem. **16**, 758 (1995).
[31] J. Mášik, J. Urban, P. Mach, and I. Hubač, Int. J. Quantum Chem. **63**, 333 (1997).